

23. R. P. Evershed, C. Heron, L. J. Goad, *Analyst* **115**, 1339 (1990).
24. P. Deines, in *Handbook of Environmental Isotope Geochemistry*, P. Fritz and J. C. Fontes, Eds. (Elsevier, Amsterdam, 1980), pp. 329–406.
25. S. E. Woodbury, R. P. Evershed, J. B. Rossell, R. E. Griffiths, P. Farnell, *Anal. Chem.* **67**, 2685 (1995).
26. H. Friedli, H. Lotscher, H. Oeschger, U. Siegenthaler, B. Stauffer, *Nature* **324**, 237 (1986).

27. We thank J. Ridge and L. Ridge for their help in providing reference fats, J. Carter and A. Gledhill for technical support, the National Environment Research Council (grant GR3/10153) for funding and MS facilities (grant F14/6/13), and English Heritage and the Northamptonshire County Archaeology Unit for archaeological samples.

3 August 1998; accepted 6 October 1998

## Pb Isotopic Variability in Melt Inclusions from Oceanic Island Basalts, Polynesia

A. E. Saal, S. R. Hart, N. Shimizu, E. H. Hauri, G. D. Layne

Previous studies have suggested that melting processes are responsible for the trace element variability observed in olivine-hosted basaltic melt inclusions. Melt inclusions from three individual lava samples (two from Mangaia, Cook Islands, and one from Tahaa, Society Islands) have heterogeneous Pb isotopic compositions, even though the erupted lavas are isotopically homogeneous. The range of Pb isotopic compositions from individual melt inclusions spans 50 percent of the worldwide range observed for ocean island basalts. The melt inclusion data can be explained by two-component mixing for each island. Our data imply that magmas with different isotopic compositions existed in the volcanic plumbing system before or during melt aggregation.

Studies of oceanic basalts have shown that the mantle is isotopically heterogeneous (1). However, the nature, distribution, and scale of these heterogeneities remain problematic. The aggregation of melts on their way to the surface, and mixing in magma chambers before eruption, can obscure the chemical and isotopic signatures of preaggregated melts. Trace and major element studies of olivine-hosted melt inclusions have been successful in defining the chemical composition of preaggregated melts. However, the lack of isotopic information in melt inclusions has made it difficult to distinguish whether these melt compositions represent different extents of melting from a single source (2) or originate from different source compositions. Here we present a study of Pb isotopes of melt inclusions from three geochemically well-characterized basalt samples (3, 4) (two from Mangaia, Cook Islands, and one from Tahaa, Society Islands chain) that reveal a large range in Pb isotopic values. The isotopic compositions of bulk samples from the Mangaia and Tahaa islands are very similar to two separate mantle compositions known as the HIMU (high-U/Pb mantle) and EMII (enriched mantle 2) end members, respectively (5). The major and trace element compositions of these lavas have been explained as resulting from melting from a single mantle source containing

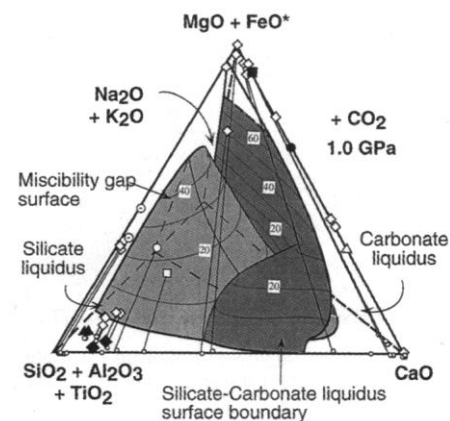
some recycled oceanic crust (6).

We recovered olivine (Fosterite content ranging from 84 to 89%) and clinopyroxene-hosted melt inclusions from two primitive basalts from Mangaia (olivines and clinopyroxenes from sample MGA-B-25, ankaramite; and olivines from sample MGA-B-47, picrite). Many of the inclusions now contain Ti-augite, Cr-spinel, ilmenite, kaersutite, sphene, apatite, and phlogopite that crystallized after entrapment of the melt (7) (see supplementary data in Table W1 at [www.sciencemag.org/feature/data/984333.shl](http://www.sciencemag.org/feature/data/984333.shl)). Some melt inclusions ( $\approx 7\%$ ) from both samples contain coexisting silicate glasses,

sulfide, and carbonate globules. These phases provide direct evidence for the existence of carbonate-rich magmas in the Cook-Austral chains, as inferred from studies of mantle xenoliths from Tubuaii (8), and of Zr/Hf fractionation in Mangaia whole-rock basalts (9). The carbonate spherules consist largely of calcium-magnesium-iron carbonate with minor alkali contents and are associated with Ca- or Mg-rich volatile-bearing silicate glasses or cryptocrystalline ground mass (up to 15% volatiles) and phonolitic glasses (Table W1). The major element compositions of the carbonates and silicate glasses from Mangaia are similar to those reported for metasomatized mantle xenoliths (for example, Spitsbergen) (10) and are inconsistent with the experimental data for liquid immiscibility (11) (Fig. 1). The phase relations shown in Fig. 1 indicate that none of the Mangaia silicate glass and carbonate globule compositions from the melt inclusions represent equilibrium immiscible liquids; they are too far removed from the miscibility gap, well inside the forbidden volumes of the primary silicate and carbonate liquidus, respectively (11). Previous work on carbonate-bearing mantle xenoliths suggested that dolomite and magnesian calcite represent primary melts, calcite is a solid phase crystallizing from a carbonated silicate melt, and amorphous magnesite-ankerite phases are formed as a result of the breakdown of primary carbonate minerals (10, 11). Mangaia silicate glasses record a complex history of crystal fractionation and probably in some cases (Mg-rich volatile-bearing glasses) decompression-induced dissolution or reaction of previously crystallized phases in volatile-rich melt inclusions (8, 10, 11). The carbonate observed in Mangaia melt inclusions crystallized from a primitive  $\text{CO}_2$ -rich magma in the lithosphere at pressures lower than 2.5 GPa (11).

The silicate glasses and carbonate globules from the Mangaia melt inclusions have a range

**Fig. 1.**  $(\text{SiO}_2 + \text{Al}_2\text{O}_3 + \text{TiO}_2) - (\text{MgO} + \text{FeO}^*) - (\text{CaO}) - (\text{Na}_2\text{O} + \text{K}_2\text{O})$  in a percent-by-weight-generalized pseudoquaternary phase diagram at 1.0 GPa (10), showing the major element composition of silicate glasses and carbonate globules from Mangaia melt inclusions and from Spitsbergen mantle xenoliths (9). The figure shows the three major liquidus volumes (the miscibility gap and the silicate and carbonate liquidus fields) and the liquidus surfaces between them. Contours and values for  $(\text{MgO} + \text{FeO}^*)$  of the surfaces are also shown as boxed numbers. Solid triangles, glass 1; solid diamonds, glass 2; dotted circle, glass 3; solid square, solid circle, and open triangle, carbonate globules; open diamonds, silicate glasses and carbonate globules from Spitsbergen xenoliths (9); open circle and open square, whole-rock lavas from Mangaia (MAG-B-47 and MAG-B-25, respectively) (4). The small circles are the projections of each point from the  $(\text{MgO} + \text{FeO}^*)$  vertex onto the basal plane of the tetrahedron. The composition of the Mangaia silicate glasses and carbonate globules is very similar to the composition of those found in Spitsbergen xenoliths. The phase relationships at 1.0 GPa (also at 2.5 GPa, not shown in figure) indicate that none of these carbonate compositions represent equilibrium-immiscible liquids. See Table W1 for supplementary data.



A. E. Saal, S. R. Hart, N. Shimizu, G. D. Layne, Department of Geology and Geophysics, Woods Hole Oceanographic Institution, Woods Hole, MA 02543, USA. E. H. Hauri, Department of Terrestrial Magnetism, Carnegie Institution of Washington, 5241 Broad Branch Road, N.W., Washington, DC 20015, USA.

## REPORTS

of trace element compositions (Fig. 2 and Table W1) (7). Silicate glasses have high Sr and Ba contents (up to 1.4 and 0.8% by weight, respectively) and variable rare earth element (REE) concentrations; La and Yb contents range from 10 to 300 and 0.3 to 20 times those of the primitive mantle (PM), respectively. Fractionation of the REEs is also large;  $(La/Yb)_{PM}$  ratios normalized to PM reach values up to 90 (most whole rocks have ratios of  $\approx 10$ ) (6), and  $Zr/Hf$  ratios are up to 100, which are typical ratios of magmas with carbonatitic affinity (9). The observed mineral associations, textures, and mineral and glass compositions in the Mangaia melt inclusions are similar to those described for carbonate-silicate melt pockets in carbonated peridotitic xenoliths (8, 11, 12).

We also recovered olivine (Fosterite content 86%)-hosted melt inclusions from a primitive basalt from Tahaa (sample TAA-B-26). All melt inclusions are ellipsoidal in shape and range from 10 to 100  $\mu\text{m}$  in diameter. In contrast to Mangaia melt inclusions, the Tahaa melt inclusions are much simpler. Silicate glasses record only in situ fractional crystallization of clinopyroxene, Cr-spinel, ilmenite, and plagioclase, and segregation of sulfide globules (Table W1). The Tahaa melt inclusions have a smaller range in REE concentrations (La and Yb ranging from 50 to 250 and 3 to 10 times those of the primitive mantle, respectively) and smaller REE fractionation ( $(La/Yb)_{PM}$  ranges from 9 to 33) than the Mangaia inclusions (Table W1).

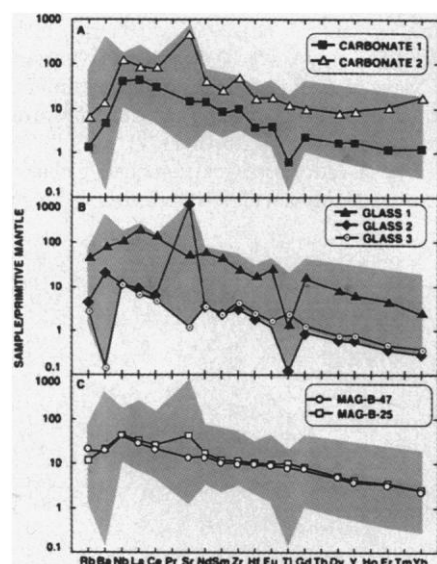


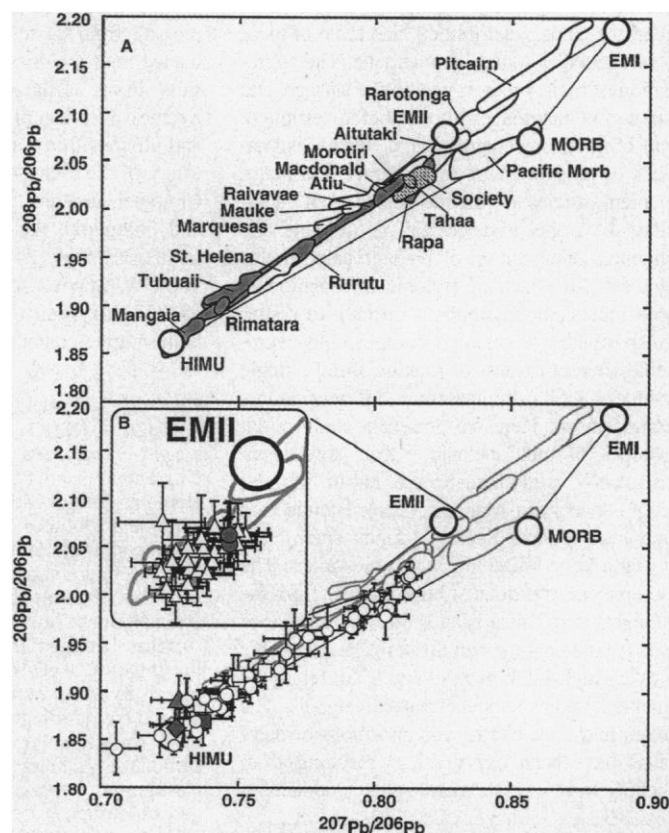
**Fig. 2.** Primitive mantle-normalized trace element data for representative melt inclusions from Mangaia. (A) Carbonates, (B) silicate glasses observed in the melt inclusions, and (C) whole-rock composition of the two Mangaia basalts (6). The shaded area defines the melt inclusion compositional range (from 46 analyses). Primitive mantle values are from (17). Symbols are as in Fig. 1. See Table W1 for supplementary data.

In Mangaia and Tahaa melt inclusions, some of the trace element variability is probably a result of partial melting processes, but much of the trace element signal is complicated by in situ fractional crystallization. In the Mangaia melt inclusions, additional complexity is added by silicate-carbonate fractionation and probably by decompression-induced dissolution or reaction of crystal phases in volatile-rich melt inclusions. Thus, although the presence of carbonates shows that the sub-Mangaia mantle is at least locally carbon-rich, the trace element data indicate little else about the Mangaia and Tahaa mantle source compositions, and it is difficult to deduce information regarding mantle source variability from the trace element compositions observed in these melt inclusions. Thus, the distinct mantle components beneath Mangaia and Tahaa are resolved by measurement of radiogenic isotopes in individual melt inclusions.

Secondary ion mass spectrometry (SIMS) analyses of Pb isotope ratios ( $^{207}\text{Pb}/^{206}\text{Pb}$  and  $^{208}\text{Pb}/^{206}\text{Pb}$ ) (13) of the melt inclusion populations from the two Mangaia basalts show large and systematic variations that overlap with the Pb isotope composition of whole rocks from the entire Cook-Austral Islands chain between Mangaia Is-

land and Macdonald seamount (Mangaia, Tubuaii, Rimatara, Rurutu, Raivavae, Rapa, Morotiri, and Macdonald) (Fig. 3, A and B) (see supplementary data in Table W2 at [www.sciencemag.org/feature/data/984333.shl](http://www.sciencemag.org/feature/data/984333.shl)). The ranges in isotopic composition ( $^{207}\text{Pb}/^{206}\text{Pb}$  varies from 0.706 to 0.815, and  $^{208}\text{Pb}/^{206}\text{Pb}$  ratios range from 1.840 to 2.02) are much larger than that observed for Mangaia whole-rock lavas (0.726 to 0.735 and 1.869 to 1.883, respectively) and cover 50% of the entire range defined by the worldwide population of oceanic island basalts (OIBs). The ranges in Pb isotopic composition of melt inclusions from Tahaa ( $^{207}\text{Pb}/^{206}\text{Pb}$  varies from 0.809 to 0.824, and  $^{208}\text{Pb}/^{206}\text{Pb}$  ratios range from 2.009 to 2.048) are larger than that observed for Tahaa whole-rock lavas (from 0.811 to 0.816 and from 2.027 to 2.032, respectively) and overlap with the Pb isotope composition of whole rocks from the entire Society Islands (Cyana, Mehetia, Moua Piha, Rocard, Tahaa, Tahiti, and Teahitia) (Fig. 3, A, B, and inset and Table W2). For samples with high Pb concentrations [measured  $^{208}\text{Pb}$  counts rates higher than 2000 counts per second (cps)], we measured  $^{206}\text{Pb}/^{204}\text{Pb}$  ratios in subsets of melt inclusions from both Mangaia and Tahaa samples. The  $^{206}\text{Pb}/$

**Fig. 3.**  $^{208}\text{Pb}/^{206}\text{Pb}$  versus  $^{207}\text{Pb}/^{206}\text{Pb}$  ratios. (A) Pb isotopic composition of whole-rock basalts from Pitcairn Island, Pacific MORB, the Society Islands, the Marquesas, St. Helena, and the Cook-Austral Islands. Shaded fields represent the Pb isotopic compositions of the islands and seamounts from the Cook-Austral chain between Mangaia Island and Macdonald seamount; dashed fields represent the Society Islands, where the field for Tahaa is highlighted [data are from (3, 5, 6, 13, 18)]. Large open circles are the four end members of the mantle tetrahedron (5) projected onto the  $^{208}\text{Pb}/^{206}\text{Pb}$  -  $^{207}\text{Pb}/^{206}\text{Pb}$  plane. (B) Pb isotopic composition (Table W2) for individual olivine and clinopyroxene-hosted melt inclusions from Mangaia basalts MAG-B-47 (open circles) and MAG-B-25 (open squares). Solid diamond, sulfide globule; solid square, carbonate globule (both from MAG-B-25); solid triangle, carbonate globule from MAG-B-47. The inset shows a magnified view of the Pb isotopic composition of individual olivine-hosted melt inclusions from Tahaa basalt TAA-B-26 (open triangles); solid circle, sulfide globule composition (Table W2). Error bars indicate in-run precision ( $2\sigma$ , standard error).



$^{204}\text{Pb}$  ratios for Mangaia and Tahaa melt inclusions range from 22.01 to 19.63 and from 18.94 to 19.73, respectively [compared with a range from 21.480 to 21.932 and from 19.16 to 19.29 in Mangaia and Tahaa whole-rock lavas, respectively (3, 5, 6)] and substantiate the variation observed in  $^{207}\text{Pb}/^{206}\text{Pb}$  and  $^{208}\text{Pb}/^{206}\text{Pb}$  ratios.

The Pb isotope data for Mangaia and Tahaa forms quasi-linear arrays that can be described by simple mixing of two end members. For Mangaia, one component is rich in radiogenic Pb and is identical to the HIMU component observed in erupted Mangaia lavas (3, 6); the Pb isotopic compositions of sulfide- and carbonate-bearing melt inclusions are invariably end-member HIMU; whether the carbonation is responsible for the HIMU signature or merely accompanies it is still an unresolved issue. The second component is defined by a less radiogenic Pb composition (hereafter called the less radiogenic component). The exact identity of this component is difficult to establish, partly because of the analytical errors involved, as can be seen from Fig. 3B; it could be either the enriched mantle component observed in erupted lavas from other islands in the Cook-Austral chain (14) (for example, Macdonald seamount) or a depleted upper mantle component [that is, Pacific mid-ocean ridge basalt (MORB)]. For the Tahaa melt inclusions, the Pb isotopic composition can also be explained by mixing between a component represented by the EMII mantle end member and a second component that is identical to the less radiogenic component observed in Mangaia melt inclusions. The Pb isotopic compositions of Tahaa sulfide-bearing melt inclusions are end-member EMII (inset, Fig. 3B). The less radiogenic component present in melt inclusions from

both of the end member OIBs is similar to ubiquitous mantle components such as FOZO (5) or C (15), although the geologic significance of this similarity is not clear.

The Pb isotope compositions in melt inclusions from sample MAG-B-47 correlate negatively with the Cr content of daughter clinopyroxene; the melt inclusions from Tahaa plot at one extreme of this correlation, corresponding to the less radiogenic component and the lowest Cr content of daughter clinopyroxene (Fig. 4). The Cr variation in daughter clinopyroxene included in the melt inclusions could be considered to reflect a different extent of in situ fractionation resulting from olivine and Cr-spinel crystallization in the melt inclusion. However, the correlation between the Pb isotopes and the Cr content in the clinopyroxene cannot be explained by simple crystal fractionation and instead requires a process that couples the change of Cr in clinopyroxene with the Pb isotope composition of the melt inclusions. This negative correlation suggests that the melt corresponding to the less radiogenic component may have suffered differentiation before its entrapment. We can explain this correlation if a HIMU melt underwent coupled assimilation and fractional crystallization or mixed with a differentiated melt (low Cr and high Pb content, with a less radiogenic signature) within the oceanic lithosphere before entrapment. The less radiogenic component could also be melt originating from a previously differentiated source (for example, eclogites produced by recycled oceanic crust). The SIMS Pb data and the range of  $\delta^{18}\text{O}$  (from 4.98 to 5.03 for Mangaia and 5.71 for Tahaa) previously measured in olivine phenocrysts from the same samples (16) suggests that the less radiogenic component could be derived either from the mantle or the oceanic lithosphere.

There exists no evidence from data on erupted Mangaia lavas for the second, less radiogenic, component that is observed in the melt inclusions. This lack of evidence in the erupted lavas as well as the higher Pb content (high Pb count rates) in the melt inclusions with less radiogenic isotopic compositions suggest that the proportion of this component in the erupted lavas must be small. In contrast, the Pb isotopic composition of whole-rock lavas from Tahaa is within errors the same as those of the less radiogenic component observed in the melt inclusions, which suggests a high proportion of this end member and the dilution of the EMII end member in the Society Islands. It is apparent from the Pb isotope data that shallow-level storage and mixing of distinct magma batches resulted in homogenization and dilution of the less radiogenic component within Mangaia magmas, and in dilution of the EMII component in the Tahaa lavas, before eruption. The melt inclusions are thus valuable samples for revealing magmatic diversity within the volca-

nic plumbing system beneath Mangaia and Tahaa and provide information that is invisible in the erupted lavas.

The broad linear trend defined by the Pb isotopic composition of melt inclusions from Mangaia and Tahaa samples reproduces the entire trend defined by the Austral and Society island chains. The inclusions preserve a record of melt composition of far greater isotopic diversity than that sampled in whole-rock analysis. The results suggest that the entire Austral chain and the Society island array can be explained by mixing of the HIMU and EMII components with a common component (the less radiogenic component), respectively. The HIMU Pb isotopic composition measured in the carbonated globules, in conjunction with their textures and compositions, provide direct evidence for a carbonated mantle source beneath the Austral Islands.

#### References and Notes

1. A. Zindler and S. R. Hart, *Annu. Rev. Earth Planet. Sci.* **14**, 493 (1986).
2. A. Sobolev and N. Shimizu, *Nature* **363**, 151 (1993); A. A. Gurenko and M. Chaussidon, *Geochim. Cosmochim. Acta* **59**, 2905 (1995); V. Kamenetsky and R. Clocchiatti, *Earth Planet. Sci. Lett.* **142**, 553 (1996).
3. E. H. Hauri and S. R. Hart, *Earth Planet. Sci. Lett.* **114**, 353 (1993).
4. ———, *Chem. Geol.* **139**, 185 (1997).
5. S. R. Hart, E. H. Hauri, L. A. Oschmann, J. A. Whitehead, *Science* **256**, 517 (1992).
6. J. D. Woodhead, *J. Volcan. Geotherm. Res.* **72**, 1 (1996).
7. N. Shimizu and S. R. Hart, *Annu. Rev. Earth Planet. Sci.* **10**, 483 (1982); E. H. Hauri, J. Zhang, C. Herzberg, Y. Fei, *J. Conf. Abstr.* **1**, 241 (1996) *V. M. Goldschmidt Conference, 1996, Heidelberg* (Cambridge Publications, Cambridge, 1996).
8. E. H. Hauri, N. Shimizu, J. Dieu, S. R. Hart, *Nature* **365**, 221 (1993).
9. C. Dupuy, J. M. Liotard, J. Dostal, *Geochim. Cosmochim. Acta* **56**, 2417 (1992).
10. D. Ionov, S. O'Reilly, Y. Genshaft, M. Kopylova, *Contrib. Miner. Petrol.* **125**, 375 (1996).
11. W.-j. Lee and P. J. Wyllie, *J. Petrol.* **39**, 495 (1998).
12. L. N. Kogarko, C. M. B. Henderson, H. Pacheco, *Contrib. Miner. Petrol.* **121**, 267 (1995).
13. Lead isotopes were determined by SIMS with a Cameca IMS 1270 ion microprobe at the Woods Hole Oceanographic Institution. We used a primary ion beam of 22.5 keV  $^{16}\text{O}^-$  and currents ranging from 30 to 50 nA, focused into a spot 20 to 30  $\mu\text{m}$  in diameter. To resolve isobaric interferences, secondary ions were analyzed at a mass resolution of 3500 with no energy filtering. Each analysis comprised 200 to 400 cycles of alternating measurements of  $^{206}\text{Pb}$  (4 s counting),  $^{207}\text{Pb}$  (4 s counting),  $^{208}\text{Pb}$  (2 s counting), and background (1 s counting). The in-run precision inversely correlates with the Pb content of the sample; the typical in-run precision for the Pb isotopic measurements ( $^{207}\text{Pb}/^{206}\text{Pb}$  and  $^{208}\text{Pb}/^{206}\text{Pb}$ ) ranges from  $\approx 0.2\%$  ( $2\sigma$ ;  $^{208}\text{Pb}$  count rates, 10,000 cps) to 1.2% ( $2\sigma$ ;  $^{208}\text{Pb}$  count rates, 200 cps). When  $^{208}\text{Pb}$  count rates were higher than 2000 cps, we also measured  $^{204}\text{Pb}$  (8 s counting), with an in-run precision for  $^{206}\text{Pb}/^{204}\text{Pb}$  ranging from  $\approx 0.5\%$  ( $2\sigma$ ; 10,000 cps for  $^{208}\text{Pb}$ ) to 1.6% ( $2\sigma$ ; 2,000 cps for  $^{208}\text{Pb}$ ). We used Loihi glass 158-4 previously analyzed by thermalization mass spectrometry (TIMS) as a standard during the period of measurement of the melt inclusions [see M. O. Garcia, D. J. P. Foss, H. B. West, J. J. Mahoney, *J. Petrol.* **36**, 1647 (1995)]. The Pb content of the Loihi glass is  $\approx 3$  parts per million (ppm), similar to the Pb content of the melt inclusions from Mangaia. Typical  $^{208}\text{Pb}$  count rates were approximately

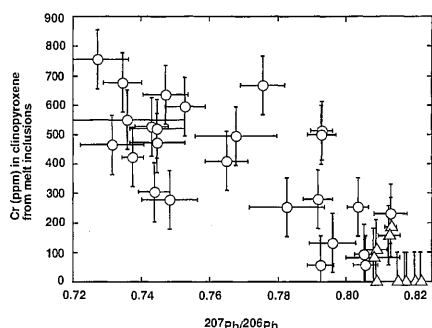


**Fig. 4.**  $^{207}\text{Pb}/^{206}\text{Pb}$  ratios for single melt inclusions versus the Cr content of included clinopyroxenes in the inclusions from Mangaia (MAG-B-47; open circles) and Tahaa (TAA-B-26; open triangles). The negative correlation suggests that the less radiogenic component suffered differentiation before entrapment by the olivine phenocrysts or that it originated from partial melting of a differentiated source [such as recycled oceanic crust (eclogite)]. The error bars for  $^{207}\text{Pb}/^{206}\text{Pb}$  ratios indicate in-run precision ( $2\sigma$ , standard errors); for Cr content, they indicate the standard deviation ( $2\sigma$ ) from replicated analyses.

400 cps per part per million of total Pb. The ion probe analyses reproduced the TIMS value within <0.1% standard errors ( $2\sigma$ ,  $n = 35$ ). The mass fractionation for SIMS analysis was <0.15% per atomic mass unit and was smaller than the in-run precision. Comparison of TIMS and SIMS Pb isotope data for basaltic glass, feldspar, chalcopyrite, and zircon indicates that instrumental mass fractionation is generally smaller than the precision of the analyses [see also G. D. Layne and N. Shimizu, in *Secondary Ion Mass Spectrometry SIMS XI*, G. Gillen, R. Lareau, J. Bennett, F. Stevie, Eds. (Wiley, New York, 1997), pp. 63–65].

14. Y. Nakamura and M. Tatsumoto, *Geochim. Cosmo-*

*chim. Acta* **52**, 2909 (1988); C. Chauvel, W. McDonough, G. Guille, R. Maury, R. Duncan, *Chem. Geol.* **139**, 125 (1997); C. Hemond, C. W. Devey, C. Chauvel, *ibid.* **115**, 7 (1994).

15. B. B. Hannan and D. W. Graham, *Science* **272**, 991 (1996).

16. J. M. Eiler et al., *Geochim. Cosmochim. Acta* **61**, 2281 (1997).

17. S.-s. Sun and W. F. McDonough, in *Magmatism in the Oceanic Basins*, A. D. Saunders and M. J. Norry, Eds. (Blackwell Scientific, London, 1989), pp. 313–345.

18. C. Chauvel, A. W. Hofmann, P. Vidal, *Earth Planet. Sci. Lett.* **110**, 99 (1992); J. C. Lassiter, E. H. Hauri, H. G. Barszczus, *Eos (Spring Suppl.)* **79**, 5378 (1998).

19. We dedicate this paper to the memory of Rafael and Niva Katzman. We thank M. O. Garcia for the Loihi samples that we used as standards during this work and W. Lee for discussion. This work was supported by NSF grants EAR-9219958 and EAR-9804891 (S.R.H.), EAR-9628749 (N.S.), and EAR-9413985 and EAR-9725351 (E.H.H.).

5 August 1998; accepted 22 October 1998

# Tankyrase, a Poly(ADP-Ribose) Polymerase at Human Telomeres

Susan Smith, Izabela Gariat, Anja Schmitt,\* Titia de Lange†

Tankyrase, a protein with homology to ankyrins and to the catalytic domain of poly(adenosine diphosphate-ribose) polymerase (PARP), was identified and localized to human telomeres. Tankyrase binds to the telomeric protein TRF1 (telomeric repeat binding factor-1), a negative regulator of telomere length maintenance. Like ankyrins, tankyrase contains 24 ankyrin repeats in a domain responsible for its interaction with TRF1. Recombinant tankyrase was found to have PARP activity in vitro, with both TRF1 and tankyrase functioning as acceptors for adenosine diphosphate (ADP)-ribosylation. ADP-ribosylation of TRF1 diminished its ability to bind to telomeric DNA in vitro, suggesting that telomere function in human cells is regulated by poly(ADP-ribosylation).

Human telomere function requires two telomere-specific DNA binding proteins, TRF1 and TRF2 (1, 2). TRF2 protects chromosome ends (3), and TRF1 regulates telomere length (4). Overexpression of TRF1 in a telomerase-expressing cell line leads to progressive telomere shortening, whereas inhibition of TRF1 increases telomere length (4). TRF1 does not control the expression of telomerase itself but is thought to act in cis by inhibiting telomerase at telomere termini.

To identify additional telomere-associated proteins, we used a yeast two-hybrid screen with human TRF1 as bait (5, 6). This screen yielded two overlapping partial cDNAs (TR1L-4 and TR1L-12) (Fig. 1A). A full-length testis cDNA isolated with TR1L-4 encoded an open reading frame of 1327 amino acids, predicting a protein of 142 kD (Fig. 1A) (7). The central domain of this protein contains 24 ankyrin (ANK) repeats, a 33-amino acid motif that mediates protein-protein interactions (8), and its COOH-terminal region has homology to the catalytic domain of PARP, a highly conserved nuclear enzyme found in most eu-

karyotes (9). We therefore named the protein tankyrase (TRF1-interacting, ankyrin-related ADP-ribose polymerase).

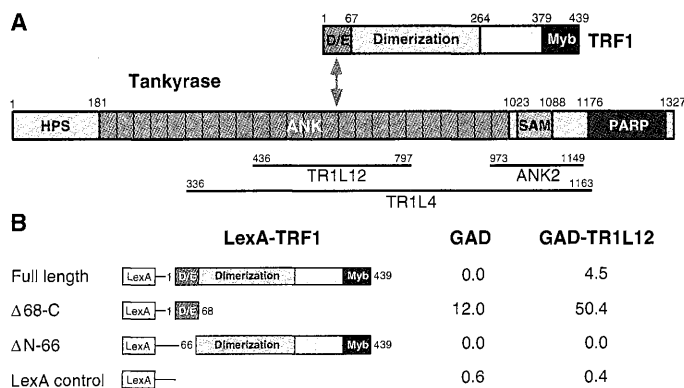
The tankyrase-interacting domain in TRF1 was identified by two-hybrid analysis (6) with TR1L-12 (Fig. 1A). The tankyrase fragment, consisting of 10 ANK repeats, interacted with full-length TRF1 but not with a TRF1 mutant lacking the NH<sub>2</sub>-terminal acidic domain of TRF1 (Fig. 1B). Consistent with this observation, significant interaction occurred with the isolated NH<sub>2</sub>-terminal 68

amino acids of TRF1, which encompass the acidic domain (Fig. 1B). These results indicate that the acidic domain of TRF1 is necessary and sufficient for interaction with tankyrase. This domain is absent from TRF2, and a two-hybrid analysis (6) indicated that tankyrase does not interact with TRF2.

Three observations suggested that tankyrase was a member of the ankyrin family, a group of structural proteins that link integral membrane proteins to the underlying cytoskeleton (10). First, tankyrase, like all ankyrins, contained 24 copies of the ANK motif, whereas other ANK repeat-containing proteins typically have 4 to 8 repeats. Second, the ANK repeats in tankyrase and the ankyrins shared characteristic sequence features, such as the presence of a hydrophobic amino acid at position 3 and an Asn or a Asp at position 29 (Fig. 2A). Third, the fifth ANK copy in tankyrase was notably shorter than all others, a feature also observed in ankyrins. Apart from the ANK repeat domain, however, there was no detectable homology between tankyrase and ankyrins. The ankyrin domain of tankyrase is flanked at the NH<sub>2</sub>-terminus by a region carrying homopolymeric His, Ser, and Pro tracts and at the COOH-terminus by a sterile alpha module (SAM) motif (Fig. 2B), which is postulated to function in protein-protein interaction (11).

The most striking feature of tankyrase is the homology to PARP. In response to DNA dam-

**Fig. 1.** Domain structure of tankyrase and two-hybrid interaction with TRF1. (A) Schematic representation of the structure of tankyrase and TRF1. Lines below the schematic indicate inserts of the two-hybrid plasmids (TR1L-4 and TR1L-12) and a plasmid used to generate recombinant protein for antibody production (ANK2). HPS, region containing homopolymeric runs of His, Pro, and Ser; ANK, ankyrin-related domain; SAM, homology to the sterile alpha motif; PARP, homology to the catalytic domain of PARP; Myb, Myb-type DNA binding motif; D/E, acidic domain rich in Glu and Asp. (B) Two-hybrid assay for the tankyrase interaction domain in TRF1.  $\beta$ -Galactosidase concentrations (Miller units; average of three independent transformations) were measured for strains expressing the indicated fusion proteins (6). GAD, GAL4 activation domain.



The Rockefeller University, 1230 York Avenue, New York, NY 10021, USA.

\*Present address: European Molecular Biology Laboratory-Heidelberg, Meyerhofstrasse 1, D-69117, Heidelberg, Germany.

†To whom correspondence should be addressed. E-mail: delange@rockvax.rockefeller.edu